Available online at www.sciencedirect.com
ScienceDirect
Journal of the European Ceramic Society 30 (2010) 2209–2221
www.elsevier.com/locate/jeurceramsoc

Tensile creep and rupture of 2D-woven SiC/SiC composites for high temperature applications

Gregory N. Morscher *

Mechanical Engineering, University of Akron, Akron, OH 44325-3903, United States

Available online 5 March 2010

Abstract

The tensile creep and rupture behavior of 2D-woven SiC fiber-reinforced SiC matrix composites with potential for advanced high temperature structural applications was determined in air at 1315 °C. The results are compared to similar SiC/SiC data in the literature in order to understand the underlying creep and rupture mechanisms. Focus was placed on three different near-stoichiometric SiC fiber-types and three SiC-based matrix systems produced by different process routes. In general, the creep and rupture properties of the tested composites were primarily dictated by the creep resistance of the fiber-type, with the Sylramic-iBN fiber typically showing the best behavior. However, the type of matrix did have an effect on the composite creep and rupture lives due to load-sharing differences for the different matrix types and due to stoichiometry in the case of chemical vapor infiltration SiC matrices.

Keywords: Ceramic matrix composites; Creep; Rupture; Mechanical properties; SiC

1. Introduction

The need for higher temperature (>1300 °C) reusable materials for advanced aero and space applications, such as hot turbine engine components, leading edge applications for hypersonic vehicles, and load-bearing TPS structures, will require advancements in ceramic composite technology. Historically, single-use hypersonic applications have relied on carbon fiber-reinforced carbon matrix or SiC matrix composites that could survive the short times (minutes) required for exit and/or entry into the atmosphere.[1] However, for multiple use re-entry applications or long-time high temperature gas turbine environments, SiC fiber-reinforced SiC matrix composites are now being strongly considered as a reusable structural material candidate.[2,3]

2D-woven composites with slurry-cast Si melt-infiltrated (MI) SiC-based matrices reinforced with polycrystalline fiber-types such as Sylramic-iBN or Hi-Nicalon Type-S have been shown to be materials capable of 1315 °C for relatively long times and moderate tensile stress levels (greater than 100 MPa).[4–6] However, for higher temperatures, such as those required for hypersonic applications, other more stoichiometric matrix systems with minimum free Si will be necessary, such as chemical vapor infiltration (CVI) derived SiC matrices, polymer infiltrated and pyrolysis (PIP) derived SiC-based matrices, or combinations thereof (CVI–PIP).[4] In addition, due to the high processing temperatures (>1600 °C) typically needed to stabilize the microstructures of the CVI and PIP matrices,[4,7,8] near-stoichiometric SiC fibers that have been produced near or above these temperatures will be required.[8,9]

Therefore, the purpose of this study was to compare the creep and rupture properties of different SiC fiber-reinforced SiC matrix composites with a view to the effects of the two major constituents, i.e., the fiber and the matrix. Some tensile creep studies have been performed on high-content CVI SiC[10–13] and PIP SiC[14] matrices for composites with lower temperature polymer-derived SiC-based fiber-types. This study will focus on composites reinforced with more creep-resistant fibers.

The approach will be to first compare the creep properties of the fibers themselves. The polycrystalline SiC fibers of interest are Tyranno SA (SA) from Ube Industries, Japan, Hi-Nicalon Type S (HNS) from Nippon Carbon, Japan, and Sylramic-iBN (iBN) from COIC/ATK, San Diego CA. This last type was developed by NASA using a proprietary heat treatment of the COIC/ATK Sylramic fiber.[9,15] Descriptions of these fiber-types can be found in Refs. 9 and 16. Although possessing the largest average grain size of the three types, which should improve its relative creep resistance, the SA fiber contains Al as a sintering aid which enhances its creep in comparison to the other fibers.

* Tel.: +1 330 972 7741.
E-mail address: gm33@uakron.edu.

0955-2219/$ – see front matter © 2010 Elsevier Ltd. All rights reserved.
doi:10.1016/j.jeurceramsoc.2010.01.030

The HNS fiber does not contain sintering aids, but has a finer grain size than SA and iBN. The Sylramic fiber has an intermediate grain size and is processed with boron as a sintering aid; however, after the NASA treatment, much of the B-containing species is removed from the fiber so that the creep properties of the resulting Sylramic-iBN fiber are much improved compared to the original Sylramic fiber.

After the fiber creep behavior is discussed, the on-axis creep and rupture properties of 2D-woven composites using the three fiber-types in a MI matrix will be examined in order to assess how the creep behavior of the composites compares to the creep behavior of the fibers themselves. For long-term use, these MI composites are considered limited to ~1315 °C due to free Si in the matrix. Finally, the creep and rupture behavior of the HNS and iBN fiber-types in three different matrix composites, MI, CVI, and PIP, will be compared in order to assess the effect of matrix type on composite creep and rupture properties. The CVI and PIP based matrices have potentially higher temperature capability than the MI-based matrix due to the absence of free Si. Thus it is hoped that this study will not only serve as a basis for SiC/SiC composite constituent composition/property understanding, but also towards development and implementation of advanced SiC/SiC composites with higher temperature capability. The results could also serve as a basis for potential SiC fiber-reinforced UHTC (Ultra High Temperature Ceramic) matrix composites. It is expected that some UHTC containing materials will require SiC fiber-reinforcement in order to attain shape fabrication and toughness requirements for various aerospace components. In fact, it is possible that UHTC composites would rely on the fiber-reinforcement described in this study if not the SiC fiber-reinforced CVI SiC skeletal structure for reinforcement.

2. Experimental

The composites compared in this study are described in Table 1. They were all produced as thin-walled panels with balanced fiber architectures made up of stacked pieces of 2D-woven five-harness satin cloth. The table is organized according to the order presented in this paper: MI composites with the three different fiber-types (SA, HNS, and iBN), and HNS and iBN fiber-reinforced composites with the CVI and PIP matrices. All of the composites were manufactured with a CVI BN interphase. As described elsewhere,[4,5] the MI matrices are first formed by deposition of ~20 vol.% CVI SiC onto the stacked preform, followed by low temperature infiltration of ~15% of SiC slurry and high temperature (~1400 °C) infiltration of ~15% molten silicon alloy into the remaining perform porosity. These MI composites were produced both by GE CCP (Newark, DE) and by Goodrich (Santa Fe Springs, CA) with no significant difference in creep or rupture behavior for the same fiber-type. Some of the data used for comparison here is taken from other studies[15,17–20] with appropriate references and some of the data are previously unpublished. The test methods and creep–rupture rig use for all composites of this study were identical to the referenced studies and are briefly described below.

Table 1
Physical and mechanical properties of CVI SiC containing composites studied.

Panel name	Thickness {# spec} ± scatter, mm	f	E, GPa	RT UTS, MPa	RT failure strain, %	Avg. failure stress of fibers at failure, MPa	0.005% offset stress, MPa	1st AE event stress, MPa	1st loud AE event stress, MPa	AE onset stress, MPa
SA3 MI[19]	2.05 {7} + 0.12	0.348 {7} + 0.02	254{1}	358{1}	0.33{1}	2000{1}	152{1}	100 {1}	129 {1}	145{1}
HNS MI 1[5,19]	2.49 {7} + 0.09	0.302 {7} + 0.012	262{1}	341{1}	0.63{1}	2278{1}	154{1}	80 {1}	134 {1}	150{1}
HNS MI 2[5,19]	2.17 {9} + 0.12	0.348 {9} 0.02	232{1}	412{1}	0.60{1}	2245{1}	147{1}	85 {1}	120 {1}	135 {1}
HNS CVI	2.72 {1}	0.277 {1}	273{1}	273{1}	0.39{1}	1974{1}	108{1}	70{1}	70{1}	79 {1}
iBN MI[8,19]	2.05{2} ± 0.14	0.389{2} ± 0.02	260{4} ± 15	468{4} ± 30	0.48{4} ± 0.03	2386 {4} ± 75	184 {4} ± 19	95 {4} ± 10	165 {4} ± 6	182 {4} ± 4
iBN CVI-H	2.11 {7} ± 0.10	0.374 ± 0.018	266{2} ± 9	440{2} ± 12	0.49{2} ± 0.07	2381 {2} ± 133	139 {2} ± 1	61 {2} ± 24	69 {2} ± 19	101 {2} ± 1
iBN CVI-G[17,20]	2.18 {3} ± 0.01	0.364 ± 0.001	242{3} ± 18	430{3} ± 6	0.52{3} ± 0.017	2363{3} ± 38	150{3} ± 5	81 {3} ± 12	118 {3} ± 9	116{3} ± 6
iBN PIP-1A	1.50 {2} ± 0.01	0.526{2} + 0.004	161 {1}	431 {1}	0.35 {1}	1623 {1}	133 {1}	–	–	–
iBN PIP-2A	1.58 {4} ± 0.05	0.502 {4} ± 0.014	150 {1}	361 {1}	0.285 {1}	1396 {1}	165 {1}	109 {1}	271 {1}	–
iBN PIP-1B	1.54 {2} ± 0	0.514 {2} ± 0	159 {1}	389 {1}	0.317 {1}	1514 {1}	158 {1}	99 {1}	163 {1}	–
iBN PIP-2B	1.58 {2} ± 0.02	0.500 {2} ± 0.006	164 {1}	317 {1}	0.274 {1}	1281 {1}	148 {1}	–	–	–

The previously unreported composite data introduced in this study were for composites with high-content (∼40 vol.%) CVI SiC and PIP matrices. Most of these panels were reinforced with iBN fiber of the same 2D-woven balanced architecture: 8 plies of 7.9 tow ends per cm, five-harness satin 2D-woven cloth. One panel was made with 2D-woven HNS and a CVI matrix with 8 plies of cloth at 7.1 tow ends per cm. The high-content CVI composites were made by two different vendors: GE CCP (Newark, DE) and Hyper-Therm Composites Inc. (Huntington Beach, CA) and because of a difference in creep behavior are referred to as "CVI-G" and "CVI-H", respectively. The "CVI-G" panel was actually used for the room temperature mechanical property study of references 17 and 20; however, creep–rupture tests were performed on specimens from that panel in this study. The CVI panel process consisted of compression tooling of 150 mm × 230 mm stacked woven cloth pieces into a preform, the CVI deposition of a BN interphase (∼0.5 μm thick), followed by CVI of SiC near 1000 °C with ∼15 vol.% of trapped porosity remaining in the final panel. Three smaller 150 mm × 75 mm were fabricated for the high-content PIP composites by ATK/COIC (San Diego, CA). For PIP processing,[7,8] a CVI BN-based coating was initially applied to a large piece of woven cloth, which was then cut to the appropriate ply size, infiltrated with two-different polymers (A and B) plus filler, stacked, and pyrolyzed at two high temperatures (−1 and −2) above 1500 °C. Polymer impregnation and pyrolysis steps were repeated several times in order to achieve a suitable density (∼2.8 g/cm^3), but with trapped final porosity of ∼10 vol.%. Properties for the four slightly different proprietary PIP matrix variations are indicated in Table 1.

Fig. 1 shows representative microstructure of the three different matrix composites reinforced with woven iBN fibers. Noted on the figures are some of the defining features of each matrix system. The MI composites possessed a deposited CVI SiC layer on the fiber/interphase preform followed by infiltration of SiC particulate and molten Si. In some cases, considerable free Si is apparent. The CVI composites possessed large trapped pores typically at open regions in the woven preform. The PIP composites possessed shrinkage cracks due to polymer conversion to a SiC-containing matrix. It should be noted that the porosity of the CVI and PIP composites are comparable (10–15%), though distributed differently, whereas the porosity within the MI composite is much less (<5%) and concentrated within the fiber bundles.

Tensile tests performed in this study are identical to those in other studies at room temperature[5,17] and elevated temperature.[5] Greater detail can be found in those references. All tests were performed on tapered dog bone specimens oriented in one of the primary fiber directions. The specimens were ∼150 mm long with 12.6 mm wide tabs and a 10-mm wide gage section. ASTM C1275 was followed for room temperature tests, which were performed on an Instron 8562 tensile machine (Instron, Ltd., Canton, MA, USA). Strain was measured with 25 mm metal "knife edge" clip-on strain gages (2.5% max strain) and wire mesh was used around the tab ends to minimize grip pressure effects. Acoustic emission was monitored and only the data that

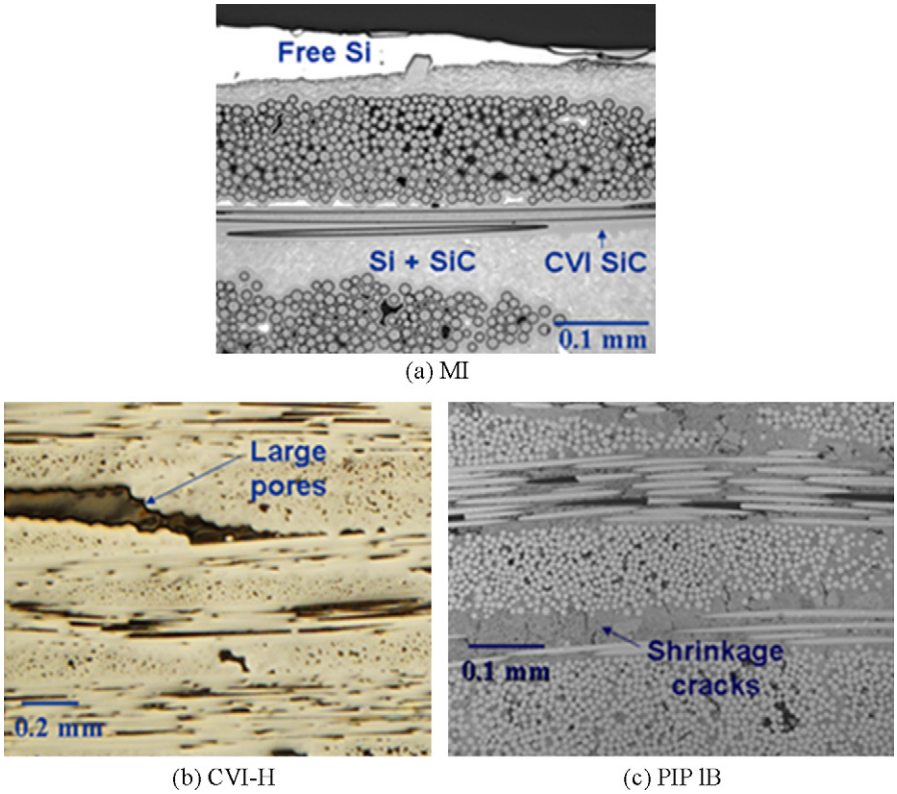

(a) MI

(b) CVI-H

(c) PIP IB

Fig. 1. Representative microstructures of the different matrix composites reinforced with Sylramic-iBN fibers.

emanated from the gage section was used in analysis. High temperature creep experiments were performed in laboratory air according to ASTM C1337 where a $MoSi_2$ resistance heated furnace was placed around the dog bone section of the composite outside of the water cooled wedge grips. A contact LVDT extensometer with SiC contacting rods (25 mm apart) and 1% strain capability was used to measure strain. Specimens were loaded at 3.23 mm/min.

Longitudinal polished sections were obtained from failed specimens. An approximately 20 mm long section from one half of the composite fracture surface was cut and polished. The specimens were polished approximately 1 mm from one of the edges, along the edge of the specimen, and low magnification optical pictures were taken to create damage maps for each specimen.

3. Results and discussion

3.1. Fiber creep data in the literature

Two approaches have been employed in the literature to determine fiber creep properties in order to understand the creep properties of different composites. One approach[16,21–23] is to perform high temperature tensile creep measurements on individual fibers for the polycrystalline SiC fibers of interest. However, with this approach, there can be complications with the temperature profile (gage length), numbers of fibers and stresses actually performed, creep strain measure, and oxidation effects. The second approach is to perform Bend Stress Relaxation (BSR) tests[24] on different fiber-types for different time–temperature conditions and often in a head-to-head manner, i.e., in the same furnace run. Though the BSR test measures relaxation at constant bend strain and not creep, it is a very simple test and has shown to be comparable to tensile creep properties for some polycrystalline SiC fiber-types.[25,26] It is also a test that offers a head-to-head comparison where all fibers can be tested at exactly the same time. However, a concern with BSR test is that it is performed in bending with maximum stress (strain) applied to the surface of the fiber so that the non-Newtonian (stress exponent > 1) behavior typically seen for tensile creep of SiC fibers complicates comparing the BSR results to the tensile creep results.

BSR data for the three fiber-types of interest are shown in Fig. 2 for 1 h tests at various temperatures.[27–29] The data is plotted as the stress relaxation ratio, m, for a 1-h isothermal exposure. All of the data was obtained in an argon environment for a furnace with graphite elements according to Ref. 24. Each data set refers to a different lot of fiber and a different series of BSR tests performed in the last few years. The stress relaxation ratio, m, is defined as the ratio of final to initial stress:

$$m = \frac{\sigma(t, T, \varepsilon_o)}{\sigma_o(t = 0, T, \varepsilon_o)} = 1 - \frac{R_o}{R_a}, \quad (1)$$

and can simply be determined by the radius the fiber is subjected to in the graphite mandrel jig, R_o, and the remaining radius after removal from the jig, R_a. If $m = 1$ (complete spring back, $R_a = \infty$), then the material behaves perfectly elastic, i.e., no time-dependent deformation. If $m = 0$ ($R_o = R_a$), then the fibers fully relaxed. Therefore, the higher the value of m for the same time/temperature conditions for a given fiber, the less stress relaxation (less creep) that occurred for that fiber when compared to another fiber-type.

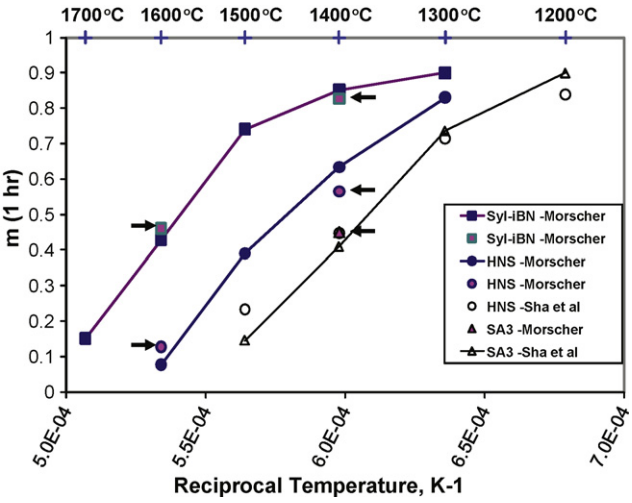

Fig. 2. BSR m ratio versus reciprocal temperature for a 1-h temperature BSR experiment with a graphite mandrel that had a radius (R_o) of 4.1 mm. The data signified by arrows indicated that these sets of data were acquired in the exact same BSR test, i.e., a head-to-head comparison under identical furnace conditions.

From the data in Fig. 2, it is evident that iBN fiber relaxed less than HNS fiber, which relaxed less than SA3 fiber. Two or three different data sets are shown for each fiber-type; some of the data from Morscher[27,29] and some of the data from Sha et al.[28] Note that for the HNS data from Sha et al. were essentially the same as for SA3; whereas HNS was superior to SA3 for Morscher. It is not understood why this is the case and may be due to different vintage fibers. However, the data with arrows in Fig. 3 are for the three different fiber-types tested at the exact same time, i.e., head-to-head, in the same jig same furnace run and show that SA3 relaxed more than HNS, which relaxed more than iBN.

Three research groups have studied the tensile creep properties of these fibers.[16,22,23] Polycrystalline SiC fibers do show a strong primary creep region and most creep experiments appear to last for only tens of hours and some for hundreds of hours. A steady state creep rate appears likely in some cases, but is not always conclusive. Some of that data are shown in Fig. 3a and b in the form of minimum strain rate at 1300 and 1400 °C, respectively. There are considerable differences between the three sets of creep data. For a given study, the SA3 creeps at a higher rate than HNS at both 1300 and 1400 °C. For the one study from Yun and DiCarlo (1400 °C), the creep rates of iBN appear to be in between SA and HNS, as well as the creep strain after 25 h (Fig. 3c), which is contrary to the BSR data.

Note that the creep rates for SA and HNS performed by Bunsell and Berger[16] are about an order of magnitude higher than the more recent study of Sauder and Lamon.[23] Bunsell, as well as Yun and DiCarlo, performed creep experiments on cold gripped fibers with resistance element furnaces in air or flowing argon, which included a significant temperature gradient along the fiber

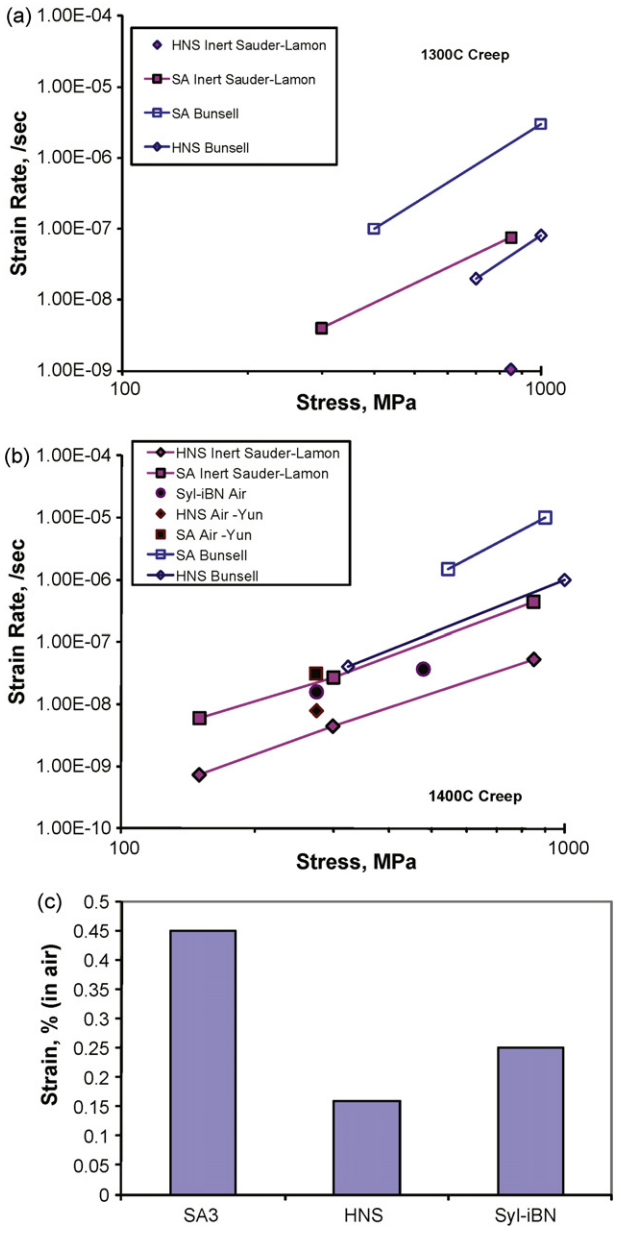

Fig. 3. Minimum strain rate data for different polycrystalline fibers at (a) 1300 °C and (b) 1400 °C; and, (c) the creep strain at 25 h for 1400C tensile creep in air at 275 MPa for the three different fibers.[16,22,23]

length, thereby requiring a length correction factor. Sauder and Lamon actually resistance heated the fibers and were able to obtain a more uniform hot zone and performed the tests in vacuum without the added complication of a receding fiber diameter due to oxidation.[1] Perhaps the variability between Bunsell and Sauder–Lamon data is due to the test technique; however, it is also very likely that the older fiber vintages tested by Bunsell were inferior compared to the more recent vintages tested by Sauder–Lamon due to further fiber processing improvements.

[1] It should be noted that Si volatilization can occur in vacuum resulting in an effective reduction in SiC fiber diameter; however, this was only significant at 1450 °C.

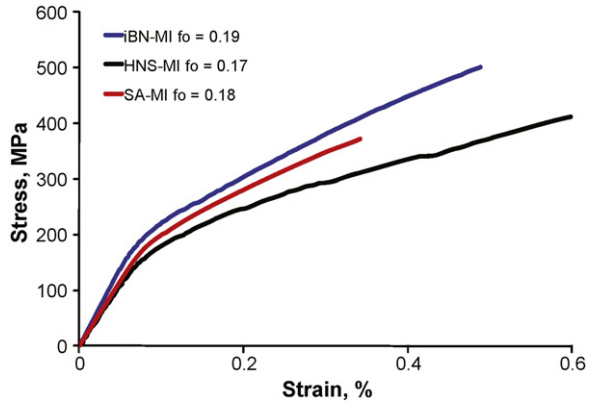

Fig. 4. Room temperature stress–strain behavior for different fiber-reinforced MI composites.

The creep data from composites in this study will be compared to the fiber data from Sauder and Lamon.

3.2. Creep comparison of woven melt-infiltrated matrix composites with different fiber-reinforcement

The mechanical properties of MI composites at room and elevated temperatures are taken from other studies.[5,18,19,30] In those studies, the focus was more on rupture behavior. Here the same data will be used; however, the creep behavior will be the focus. The rupture behavior will be compared with the other different matrix composites below.

Some room temperature stress–strain curves are shown in Fig. 4 for representative MI composites reinforced with the three different fiber-types. The composites are of slightly different fiber volume fractions. The "f_o" refers to the fraction of fibers in the loading direction, i.e., one half the total fiber volume fraction for these balanced composites. Some mechanical property data from room temperature tensile tests are listed in Table 1 for some of the different composites. Of note are the matrix cracking parameters: 0.005% PL, AE onset stress, and first AE event stress. The 0.005% PL refers to a typical designation for "proportional limit" and is determined by the intersection of a line parallel with the initial loading curve (a slope of E) displaced by 0.005% with the stress–strain curve. The AE onset stress is when high energy acoustic emission events occur and correspond to large matrix crack, if not through-the-thickness, formation occurs. The first AE event stress corresponds to the stress at which the very first AE event, typically low in energy, is detectable and usually corresponds to initial tunnel microcrack formation in the fiber tow minicomposites perpendicular to the loading direction. Typically, the PL stress is considered to be a maximum design stress; however, for high temperature stress–rupture lives, it is necessary to operate well below PL stress and perhaps even below first AE event stress if very long times are desired (>1000 h).[30] Also, all of the creep data shown in this paper are essentially at or above the first AE event stress which indicates that at least tunnel cracking can be expected to occur during loading and creep.

Typical tensile creep curves are shown in Fig. 5a.[5] Note that a constant creep rate is probably not achieved for these composites

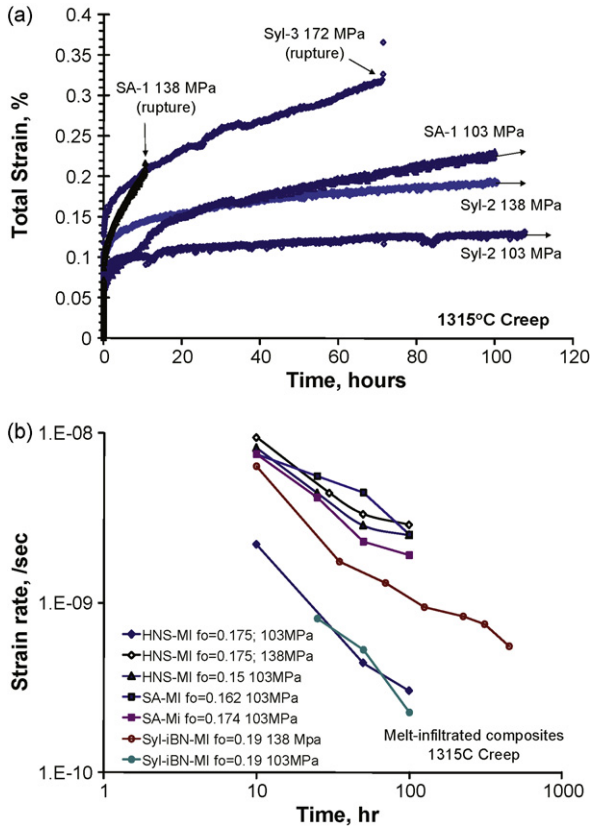

Fig. 5. (a) Typical creep curves for MI composites with different fibers from Refs. 5 and 19 and (b) instantaneous strain rates for different specimens and stresses at 1315C.

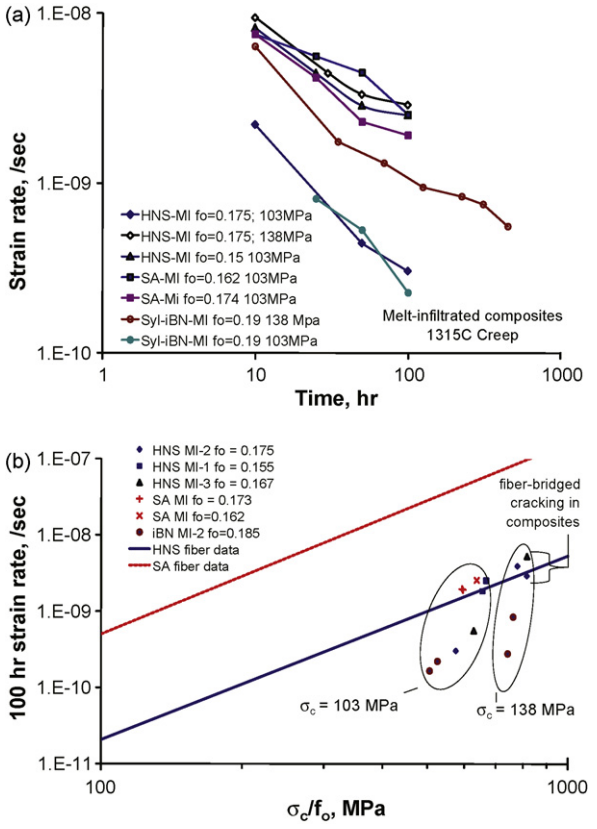

Fig. 6. Comparison of creep strain rate at 100 h for (a) individual composite specimens based on applied composite stress and (b) composites assuming the maximum stress on the fibers (σ_c/f_o) compared to estimated fiber creep rates based on fiber tensile creep at 1300 and 1400 °C from Sauder and Lamon.[23]

(Fig. 5b). However, in order to compare the composite properties to the fiber properties, the creep rate of the composites at 100 h will be used. Fig. 6a shows the creep rate versus composite stress for composites that survived at least 100 h. Note that only two stresses were tested which met this condition, 103 and/or 138 MPa for the composites compared here. For the iBN MI composite, the stress dependence was ~3.1. For the HNS composites, the stress dependence was ~8. However, the HNS MI composites tested at 138 MPa were observed to possess several fiber-bridged matrix cracks perpendicular to the applied stress that were not through-the-thickness but were at least two plies (fiber-bridged and in some cases fiber failure had occurred in the crack wake) in depth.[19] For the HNS MI and SA3 MI composites tested at 103 MPa and for iBN MI at 103 and 138 MPa, only 90° tunnel cracks or surface 90° cracks that did not extend through load-bearing fibers were observed. Undoubtedly, the increased matrix damage and possible internal oxygen attack contributed to the high strain rate for creep of HNS MI.

An extreme of creep in a MI composite would be that the matrix has significantly poorer creep properties so that all of the load originally carried by the matrix is quickly shed to the fibers. Therefore, to compare fiber creep to composite creep, it was first assumed that after 100 h, all the composite stress was on the fibers so that the maximum stress on the fibers can be determined by dividing the composite stress, σ_c, by f_o. This maximum fiber stress and associated composite 100 h creep rate are compared with the single fiber creep rate estimates in Fig. 6b. Since the tensile creep of the composites was performed at 1315 °C and the fiber creep results were obtained at 1300 and 1400 °C, fiber creep strain rate behavior at 1315 °C was estimated from the stress exponents and activation energies determined in Sauder and Lamon.[23] The actual composite stresses, 103 or 138 MPa, are noted on Fig. 6b. Due to the fact that different composites had different fiber volume fractions (Table 1), the maximum fiber stresses range in σ_c/f_o. In general, the creep ranking for composite creep of the melt-infiltrated composites based on fiber-type is as follows: SA < HNS ≤ iBN, which is consistent with the BSR data ranking. Also, at least for the lower composite stress data where little cracking had occurred in the composites, the creep rates of the fibers are significantly higher than that of the composites. This implies that after 100 h the matrix is still carrying part of the composite load. Thus a more complicated analysis is required for prediction of MI composite strain rate after 100 h at 1315 °C.[31–33] Interestingly, the strain rates for the 138 MPa HNS composites with fiber-bridged matrix cracks were near the fiber data from Sauder and Lamon.

3.3. Creep comparison of different matrix composites with woven Sylramic-iBN and HNS fiber-reinforcement

The room temperature stress–strain behavior and acoustic emission results for representative specimens from iBN

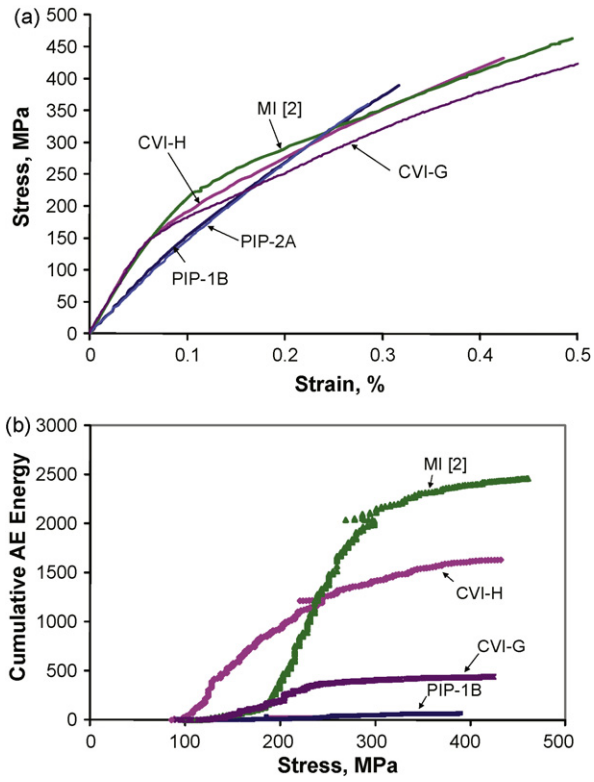

Fig. 7. Typical (a) room temperature stress–strain curves and (b) acoustic emission energy data from the gage section for the Syl-iBN CVI SiC and Syl-iBN PIP SiC composites of this study as well as a representative Syl-iBN MI SiC composite of the same fiber architecture.[18] It should be noted that the CVI-G AE was taken with a lower pre-amplification setting than the other three composites. The unload–reload loops are removed for clarity.

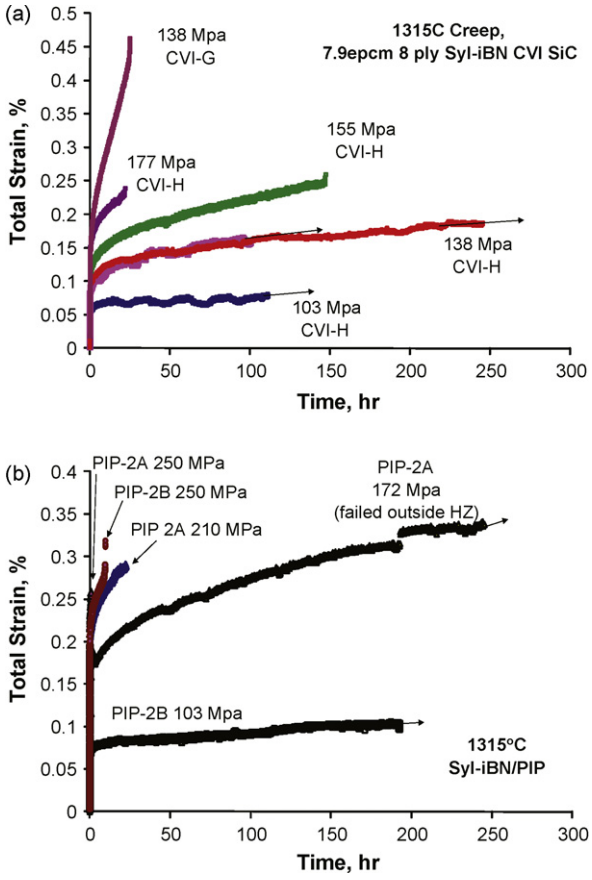

Fig. 8. Creep curves at 1315 °C for Sylramic-iBN composites with (a) CVI SiC and (b) PIP SiC matrix.

fiber-reinforced CVI and PIP composite panels as well as an iBN MI composite with the same architecture[5] are shown in Fig. 7. The iBN CVI and iBN MI composites have a high initial modulus and a sharper transition from linearity to non-linearity, i.e., proportional limit, which is indicative of significant matrix cracking in the composite with increasing stress. The non-linearity in the stress–strain curves for iBN CVI and iBN MI matrix composites are also associated with the measure of AE energy from the gage section, i.e., significant matrix crack formation. However, the iBN PIP matrix composite is lower in elastic modulus and actually is mildly parabolic (non-linear) from initial loading. Note that the AE activity in the iBN PIP matrix is much lower in energy than the other matrix systems. These types of composite behavior have been described by Evans and Zok[34] as "matrix-dominated" and "fiber-dominated", respectively. Matrix-dominated composites are composites where the matrix carries significant load at lower stresses and then demonstrates significant non-linearity with matrix cracking and local shedding, at and around matrix cracks, of load to the reinforcing fibers, e.g., CVI and MI composites of this study. Fiber-dominated composites are composites where the matrix does not carry significant stress and displays mild deviation from linearity when oriented in along one of the orthogonal fiber axes, e.g., PIP composites of this study. For the PIP composite, the matrix is heavily microcracked due to crystallization and shrinkage processes of the multiple polymer pyrolysis and densification steps during fabrication (Fig. 1).

One simple way of illustrating whether a composite is matrix-dominated would be to determine the modulus of the effective matrix (interphase, matrix, porosity, and 90° fiber tows), using the rule-of-mixtures:

$$E_{eff-mat} = \frac{E_c - f_o E_f}{1 - f_o}, \tag{2}$$

where $E_f \sim 380$ GPa for the iBN fiber. From Table 1 and Eq. (2), the effective modulus of the composite carrying load other than the load-bearing fibers ($E_{eff\text{-}mat}$) for the iBN PIP composites are about 85 GPa compared to ~250 and 225 GPa for the iBN CVI and iBN MI composites, respectively. In other words, little load is carried by the matrix for iBN PIP at initial loading of the composite, and more load carried by matrices of the other composites.

Examples of tensile creep curves are shown in Fig. 8 of the different composites at 1315 °C. The data is plotted as total strain in Fig. 8 which includes the elastic and time-dependent components of strain. Most of the curves show a continuously decreasing creep rate with a couple specimens that approach a steady state condition (Fig. 9a). For some of the longer time data, the strain rate at 100 h and the creep strain (total strain – σ/E) at 100 h are plotted versus stress in Fig. 9b. The stress exponent ($\dot{\varepsilon} \alpha \sigma^n$) for the 100-h creep rate is ~4.3 for both CVI and PIP

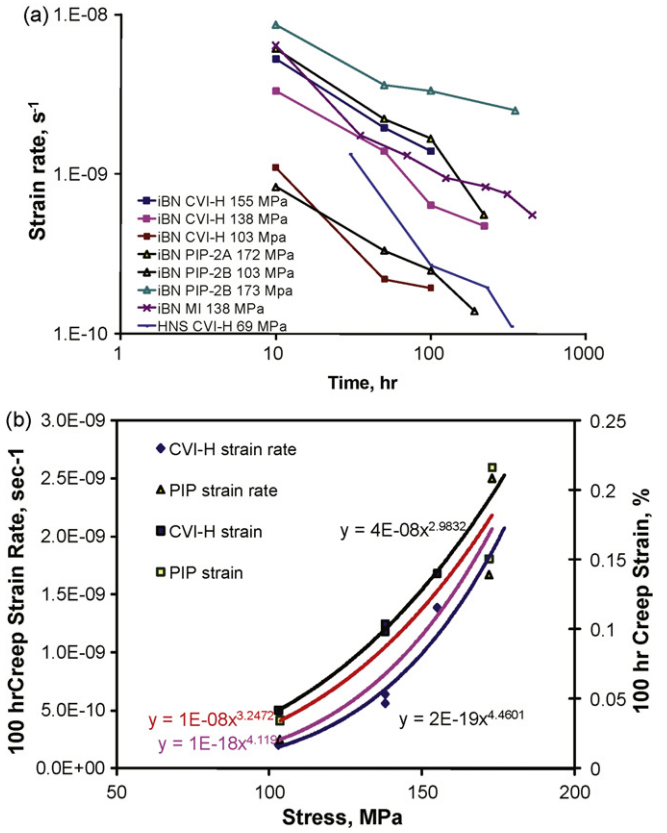

Fig. 9. (a) Creep rate for all the composites tested and (b) stress dependence of 100 h creep rate and creep strain for longer time creep data with power law best fits for two composite systems.

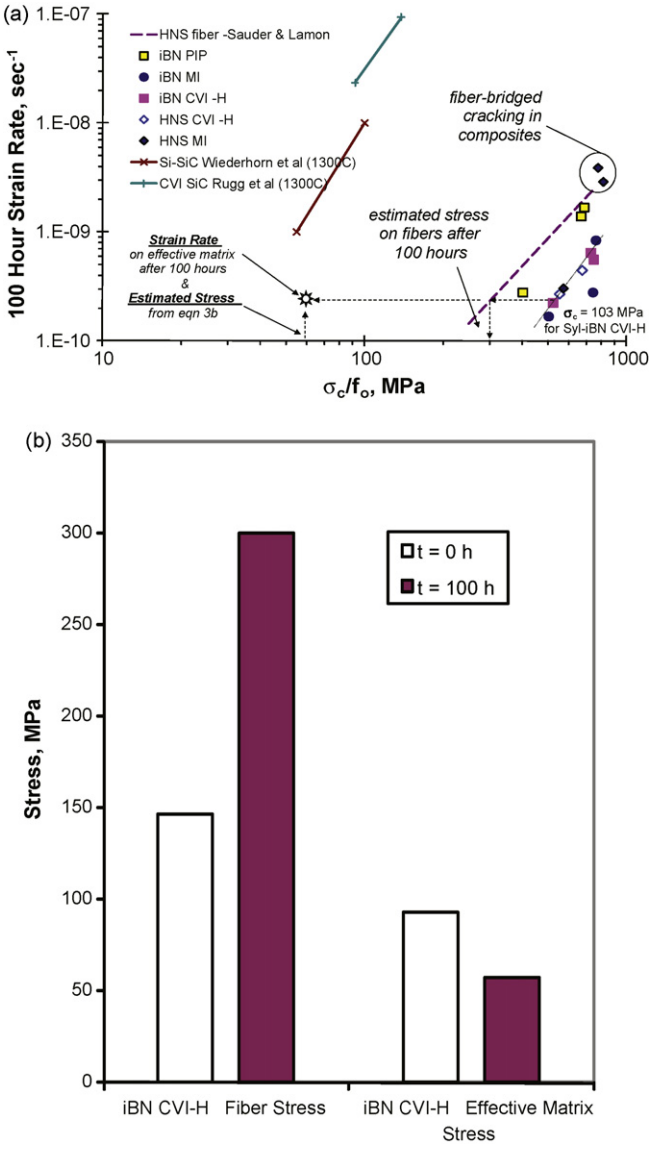

Fig. 10. (a) Creep rate at 100 h for different fiber and different matrix composites and (b) the estimated change in load sharing between fiber and effective matrix for iBN CVI-H crept at 103 MPa. For (a), the monolithic data corresponds to the applied tensile stress.

composites and the stress exponent for the 100-h creep strain is ~3. The stress dependence observed for creep of the composites is higher than that for Sylramic-iBN fibers, ~2,[21] or for other polycrystalline SiC fiber-types, ~2.5.[23] The high stress exponent for creep must be related to load sharing between fiber and matrix and stress (time) dependent matrix crack accumulation and growth (described below).

A comparison of 100 h strain rates for some of the different composites with iBN and HNS fibers plotted as σ_c/f_o are shown in Fig. 10a in order to compare to the HNS fiber data from Sauder and Lamon. As shown earlier for MI composites, iBN composite creep behavior is very similar to HNS creep behavior, if not slightly more creep resistant. Therefore, due to the lack of Sylramic-iBN fiber creep data and the similarity in composite behavior between iBN and HNS MI composites, the individual HNS fiber data from Sauder and Lamon will be treated as the fiber data to compare to.

The creep rates of the iBN PIP matrix composite are significantly higher than the CVI-H or MI matrix composites when composite stress is divided by f_o and do approach that of the fiber creep rate. Since the effective modulus of the iBN PIP composite is so low, it is not surprising that the composite data approaches the fiber data when plotted this way. Very little noticeable change was observed in the microstructure for iBN PIP composites for the various creep conditions. Fig. 11 shows some higher magnification images of the only real difference observed in some surface 90° tow minicomposites, opening of pre-existing shrinkage cracks in the matrix. There was no real discernable difference between the interior of composites after creep and for as-produced composites. Thus it is possible that after normalization of the stress by the fiber fraction, the creep rate of the iBN PIP composite after 100 h at 1315 °C shown in Fig. 9b may actually be more representative of iBN fiber creep behavior under the same stress and temperature conditions than that estimated from limited single fiber tensile data.

There is a noticeable difference between iBN CVI-G and iBN CVI-H composite creep behaviors at 138 MPa applied stress (Fig. 8a). The iBN CVI-G composite failed after only 25 h at a relatively large strain value whereas the iBN CVI-H composite did not fail after 250 h of creep before the test was stopped and the specimen was removed. For 155 MPa applied stress, the iBN CVI-G composite only survived 1.7 h (not shown); whereas the

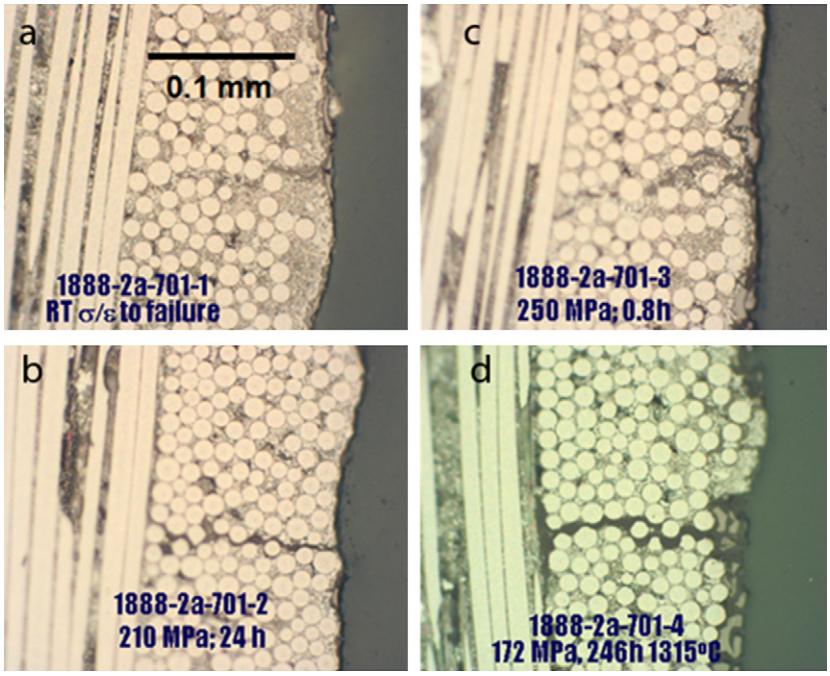

Fig. 11. The only real difference in microstructure for iBN PIP composites was opening of surface 90° pre-existing shrinkage cracks with creep time. The stress was applied in the vertical direction.

iBN CVI-H composite ruptured in creep after 147 h. These two composites are nearly the same in volume fraction; therefore, some difference in matrix properties must be the cause for the different creep behavior. The nature of matrix cracking and crack growth that occurs during creep for iBN CVI-G and iBN CVI-H composites are shown in Fig. 12 with higher magnification images of matrix cracks in Fig. 13. Cracks typically emanate from the sharp corner regions (Fig. 13) associated with the large pores.[12,35,36] It is apparent that as composite stress was increased the number of cracks and the depth of the cracks increased. For the iBN CVI-G composite, more cracking occurred as well as what appears to be the linkage of cracks to form networks of through-thickness matrix cracks at 138 and 155 MPa. However, for the iBN CVI-H composite, fewer cracks were evident at 138

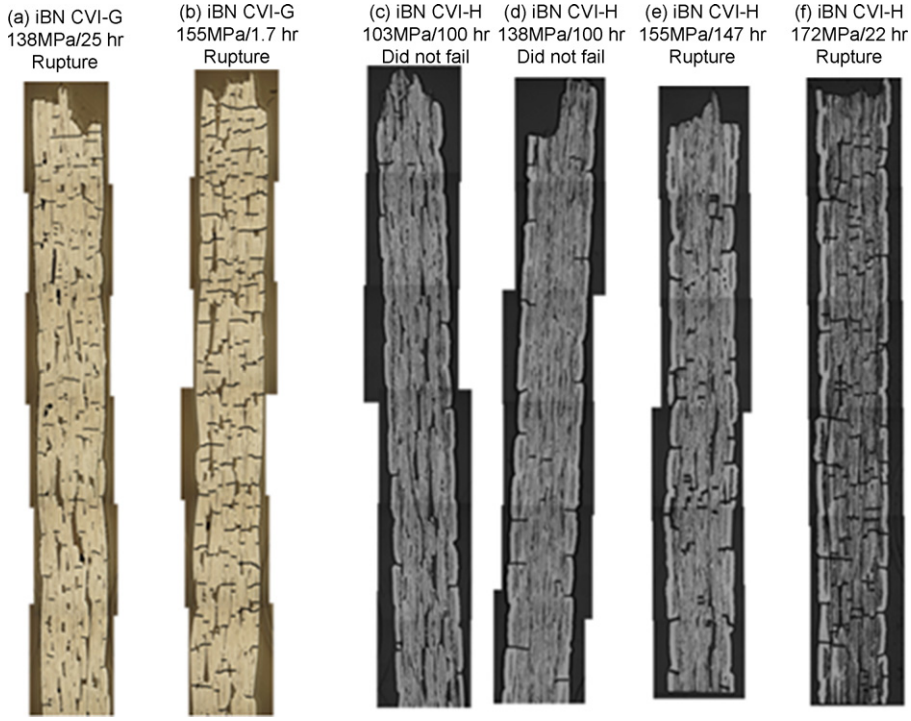

Fig. 12. Low magnification edge-cut views of crept specimens with matrix cracks emphasized by lines drawn over cracks.

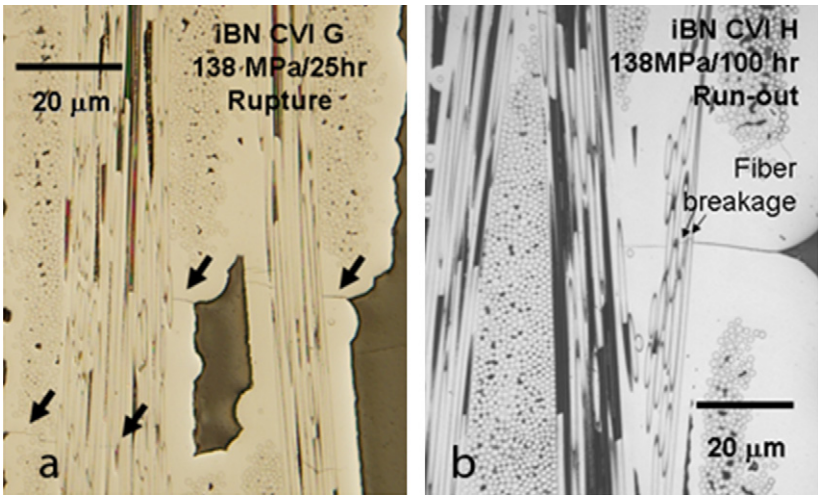

Fig. 13. Typical matrix cracks for (a) an iBN CVI-G composite and (b) an iBN CVI-H composite.

and 155 MPa compared to iBN CVI-G and no real through-thickness cracks were formed except perhaps for the higher stress condition. One difference in matrix properties was determined from Raman spectroscopy.[37] It was evident that the CVI SiC matrix for CVI-G composites was Si rich; whereas the CVI SiC matrix for CVI-H was essentially stoichiometric.[37] Silicon rich CVI is known to be more creep-prone than stoichiometric or carbon rich CVI SiC.[38] The CVI matrix results suggest that it may also be more susceptible to matrix cracking and/or slow crack growth at elevated temperature as well.

It is interesting as shown in Fig. 10a that the creep rates for iBN CVI-H, iBN MI, HNS MI at low stress, and HNS CVI-H are about the same when plotted versus σ_c/f_o, even though the MI matrices contain significant fractions of free Si (~10–15% of total composite volume) and the HNS CVI-H composite has a significantly lower fiber volume fraction. Since the strain rates for the CVI-H and MI composites at the same σ_c/f_o values are significantly lower than the PIP composites (Fig. 10a), it can be assumed that significant load sharing is occurring during creep with the matrix carrying appreciable load in these systems, although decreasing with time.

To illustrate the change in load sharing during creep, one can assume that the individual fiber strain rate corresponds to the stress in the fibers to cause that strain rate.[2] Then, the load shared by the fibers and the effective matrix can be estimated from Fig. 10a. The initial load sharing at time $t = 0$ can be estimated assuming that the composite and constituents are at equivalent strains and rule of mixtures (Eq. (2)):

$$\sigma_f = E_{f(1315C)} \frac{\sigma_c}{E_{c(1315C)}} \tag{3a}$$

$$\sigma_{eff-mat} = E_{m(1315C)} \frac{\sigma_c}{E_{c(1315C)}} = \frac{\sigma_c - f_o \sigma_{f(1315C)}}{1 - f_o} \tag{3b}$$

[2] This is inaccurate because fiber and matrix creep possess a significant primary component, the stress exponents are non-linear, and the stress states in the fibers are varying with time; however, this assumption does serve for illustrative purposes.

where the modulus at 1315 °C, $E_{(1315C)}$, for fibers and composites (Table 1) is assumed to be 10% lower than the room temperature E. Then at time $t = 100$ h, $\sigma_{f(1315C)}$ can be derived from the stress required to cause the strain rate in the fibers from the fiber data (see the construct in Fig. 10 for 103 MPa) and used in Eq. (3b) to determine the $\sigma_{eff\text{-}mat}$ at 100 h. For a 103 MPa applied stress to the composite, the stress on the fibers in Syl-iBN CVI-H with $f_o = 0.19$ would be ~147 MPa at $t = 0$ and ~300 MPa after 100 h whereas the $\sigma_{eff\text{-}mat}$ would be ~93 MPa at $t = 0$ and ~58 MPa after 100 h. This is shown graphically in Fig. 10b. One can then estimate the strain rate of the matrix from $\sigma_{eff\text{-}mat}$ as shown in Fig. 10a. Strain rates from literature data for CVI SiC measured at 1300 °C by Rugg et al.[33] and a bulk siliconized SiC (37% Si) tested in tension by Wiederhorn et al.[39] are shown on Fig. 10a for comparison. It should be noted that the CVI SiC data appears to not have reached a steady state and minimum strain rate data was used from the two CVI SiC matrix creep curves of Ref. 33. It can be seen that the data for the CVI SiC and siliconized SiC are very similar in creep, which may be why the iBN CVI and iBN MI composite data are so similar in strain rate when normalized by fiber fraction. The strain rate estimated for the effective stress on the matrix based on Eq. (3b) is reasonable (within an order of magnitude) considering the lower temperature for the bulk creep data and the variations between the actual matrix composition and bulk materials tested. Finite element approaches would be needed to accurately determine the load sharing during creep[32] provided fiber creep behavior is well characterized.

This exercise may help explain the response of the composite to matrix cracking. Compare the initial stresses for low stress AE in Table 1 to the actual applied stresses for creep. For all cases, matrix cracks would be expected to occur during the relatively rapid loading of the creep test. In fact in Ref. 18 it was shown that the crack density for 1200C creep and/or fatigue conditions was comparable to the stress-dependent crack density at room temperature for iBN MI composites and similar observations were made for MI composites with different fibers tested at 1315C.[5] However, matrix cracks were rarely observed to grow beyond one or two plies along the length of the specimen

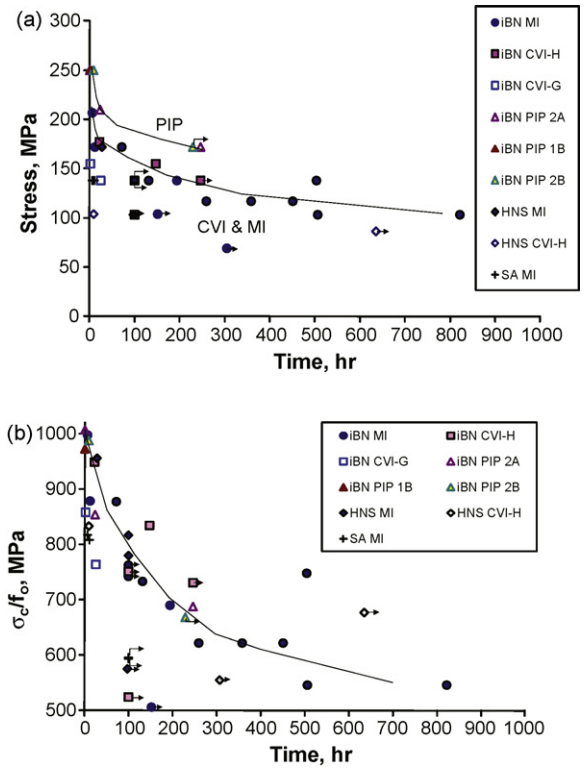

Fig. 14. Creep rupture data for (a) composite stress versus time and for (b) effective stress on fibers (composite stress divided by volume fraction in loading direction) versus time. Arrows indicate that the specimen did not rupture.

(with the exception of the one ultimate failure crack) even after long periods of times. Since load continues to be shed from the matrix to the fiber during creep (Fig. 10b), it is not surprising that general matrix crack growth is halted during creep since matrix stress unloading would continue to reduce the stress on the crack tip. Microcracks which do ultimately grow and lead to composite rupture were usually initially exposed to the environment, i.e., a surface crack, which resulted in strongly bonded fibers due to oxidation of the fibers, interphase, and matrix.[18] When a strongly bonded fiber fails in the oxidized crack wake, all the locally strongly bonded fibers fail, which in turn raises the stress in the remaining fibers and matrix sufficient for further crack propagation or microcrack linkages.[18,30]

3.4. Stress-rupture comparison of different fiber composites

The stress-rupture behavior of the composites is shown in Fig. 14a. The PIP composites were superior in stress-rupture properties compared to the CVI and MI composites. The PIP composites also had a higher fiber volume fraction. If the composite stress is divided by the volume fraction of fibers in the load direction (f_o), the rupture data for the composites are very similar (Fig. 14b), with two exceptions, the iBN CVI-G and SA MI. As discussed above, the CVI-G matrix composites had high through-thickness matrix crack densities which contributed to higher creep strains and creep rates compared to the CVI-H matrix and apparently also the shorter failure times. The SA fiber-containing composites would be expected to be inferior based on the fibers themselves being less creep resistant compared to the other fiber-types.

For the wide range of iBN and HNS composite data it is somewhat surprising that the rupture properties follow the same time dependence for σ_c/f_o given the wide range in fiber volume fractions and effective matrix moduli. For these composite systems, this implies that the creep rupture properties are primarily dictated by the fiber rupture properties. Consequently, increasing the fraction of fibers in the loading direction is expected to improve creep rupture properties for this 2D five-harness lay-up fiber architecture as well as other fiber architectures.[30] In addition, further improvements to fiber creep and rupture properties[40] should also result in improved composite and rupture properties.

4. Summary and conclusions

For the specific composites and specific test conditions used in this study, the dominant factor controlling tensile creep and rupture properties of the composites were the creep and rupture properties of the fibers. The iBN and HNS fiber-reinforcement enabled the most creep resistance compared to the SA3 fiber-type at 1315 °C. This was expected based on single fiber bend stress relaxation (BSR) and tensile creep behavior. However, it appears that the iBN composite is slightly more creep resistant at 1315 °C than the HNS, which is consistent with the BSR data of the fibers. More tensile creep data of the different fiber-types, and especially iBN, over wider stress, temperature, and time ranges is needed in order to make a clear comparison between composite and fiber data as well as to effectively model composite creep and rupture.

When normalized for fiber volume fraction, 100 h creep strain rates were significantly higher for PIP matrix composites than the MI or CVI composites and much closer to individual fiber creep data. This was expected since the PIP matrix is microcracked and thus cannot carry significant elastic and creep loads in comparison to the MI and CVI matrices, which both contain a dense minimally cracked matrix. Nevertheless, for MI and CVI composites matrix microcracks were observed for the lowest applied stress conditions (~100 MPa) of this study which was not surprising since this stress typically exceeded the lowest stress for the formation of matrix microcracks from room temperature acoustic emission findings. The formation and growth of some if not most matrix microcracks emanated from the surface of the specimen. Even so, rupture lives in excess of 500 h were observed for iBN and HNS reinforced CVI and MI composites for the 100 MPa stress state. Through-thickness matrix cracking was not observed in specimens for stresses where creep lasted over 100 h. In fact, with the exception of the final failure crack, cracks rarely grew beyond one or two woven plies. It is believed that microcracks initially form upon loading (similar to fast fracture type tests in accord with the AE data); however, since the matrix is less creep resistant than the fibers, stresses are relaxed at the crack tip with time and matrix crack growth is halted until fiber breakage of oxidized fibers occurs in a matrix crack wake. Creep-induced damage in PIP composites was negligible for creep at 1315 °C with the exception of pre-existing

shrinkage crack opening in surface tows that were perpendicular to the direction of stress.

Even though there was significant difference in load sharing, matrix cracking, and consequently strain rates for MI and CVI matrix composites compared to PIP matrix composites, the rupture times for these three composite types were similar for composite stresses normalized by the fiber fraction in the loading direction when reinforced with the iBN fiber-type. The mechanism for damage that would explain this behavior would be fiber breakage (enhanced by oxidation) in a given matrix crack and/or multiple fiber or tow breaks in (or near) a crack which would ultimately lead to unbridged crack growth and the final failure crack. Therefore, in order to achieve higher use-stress conditions will require fibers with improved creep resistance and/or higher fiber volume fractions in the direction of stress. The only exceptions to the above were the inferior rupture properties for SA fiber-containing composites due to the poorer rupture properties of the fibers themselves and CVI-G matrix composite for which the SiC matrix appeared to be silicon rich and possessed through-thickness matrix cracks at relatively low stresses when compared to the other near-stoichiometric CVI-H SiC matrix.

It should be noted that a true steady-state strain rate condition was never achieved for the composites tested in this study. This is not too surprising considering the strong primary creep component of the fibers themselves and the stress transfer from matrix to fibers during creep for these composites.

Acknowledgments

Most of this work was sponsored by NASA under several programs including ARMD Supersonics and Hypersonics programs as well as an internal IR&D program at NASA Glenn Research Center while I was employed by Ohio Aerospace Institute. I owe a debt of gratitude to Dr James DiCarlo and Doug Kiser of NASA Glenn, Dr. Ram Bhatt of the US Army, and Dr. Hee-Mann Yun of Matech GSM for materials, support and discussions. Dr. Jeff Eldridge performed the Raman spectroscopy. I especially wish to thank Ron Philips at NASA Glenn for his support in running the tensile creep rigs.

References

1. Leleu F, Watillon P, Moulin J, Lacombe A, Soyris P. The thermo-mechanical architecture and TPS configuration of the pre-X vehicle. *Acta Astronaut* 2005;**56**:454–64.
2. Naslain R. Design, preparation and properties of non-oxide CMCs for application in engines and nuclear reactors: an overview. *Comp Sci Technol* 2004;**64**:155–70.
3. Norris G. Weight revolution, GE pushes for a breakthrough in lighter materials on back of JSF F136 engine. *Aviat Week Space Technol* March 9, 2009:36.
4. DiCarlo JA, Yun H-M, Morscher GN, Bhatt RT. SiC/SiC composites for 1200 °C and above. In: Bansal NP, editor. *Handbook of Ceramics Composites*. NY, NY: Kluwer Academic; 2005. p. 77–98.
5. Morscher GN, Pujar V. Creep and stress–strain behavior after creep for SiC fiber reinforced, melt-infiltrated SiC matrix composites. *J Am Ceram Soc* 2006;**89**:1652–8.
6. Corman GS, Luthra KL. Silicon melt infiltrated ceramic composites (HiPerComp^{TM}). In: Bansal NP, editor. *Handbook of Ceramics Composites*. NY, NY: Kluwer Academic; 2005. p. 99–115.
7. Yun HY, DiCarlo JA, Bhatt RT. Advanced SiC/SiC ceramic composites for airbreathing and rocket propulsion engine components. In: *Proceedings of JANNAF Conference*. 2005.
8. Jones RE, Petrak D, Rabe J, Szweda A. Sylramic^{TM} SiC fibers for CMC reinforcement. *J Nucl Mater* 2000;**283–287**:556–9, see also www.coiceramics.com/nonoxidepg.htm [accessed July 1, 2009].
9. DiCarlo JA, Yun HM. Non-oxide (Silicon Carbide) fibers. In: Bansal NP, editor. *Non-oxide (Silicon Carbide) fibers. Handbook of Ceramic Composites*. Boston: Kluwer Academic; 2005. p. 33–52.
10. Zhu S, Mizuno M, Kagawa Y, Cao J, Nagano Y, Kaya H. Creep and fatigue behavior in Hi-Nicalon^{TM}-fiber-reinforced silicon carbide composites at high temperatures. *J Am Ceram Soc* 1999;**82**:117–28.
11. Zhu S, Mizuno M, Kagawa Y, Mutoh Y. Monotonic tension, fatigue and creep behavior of SiC-fiber-reinforced SiC-matrix composites: a review. *Comp Sci Technol* 1999;**59**:833–51.
12. Chermant JL, Boitier G, Darzens S, Farizy G, Vicens J, Sangleboeuf JC. The creep mechanism of ceramic matrix composites at low temperature and stress, by a material science approach. *J Eur Ceram Soc* 2002;**22**:2443–60.
13. Darzens S, Chermant JL, Sangleboeuf JC. Advantages of SiC Hi-Nicalon or NLM 202 fibers in SiCf–SiBN composites. *J Am Ceram Soc* 2005;**88**:1967–72.
14. Ogasawara T, Ishikawa T, Ohsawa Y, Ochi Y, Zhu S. Tensile creep behavior and thermal stability of orthogonal three-dimensional woven Tyranno^{TM} ZMI fiber/silicon–titanium–carbon–oxygen matrix composites. *J Am Ceram Soc* 2002;**85**:393–400.
15. Yun HM, Gyekenyesi JZ, Chen YL, Wheeler DR, DiCarlo JA. Tensile behavior of SiC/SiC composites reinforced by treated Sylramic SiC fibers. *Ceram Eng Sci Proc* 2001;**22**:521–31.
16. Bunsell AR, Berger MH. Fine diameter ceramic fibres. *J Eur Ceram Soc* 2000;**20**:2249–60.
17. Morscher GN, Singh M, Kiser JD, Freedman M, Bhatt R. Modeling stress-dependent matrix cracking and stress–strain behavior in 2D woven SiC fiber reinforced CVI SiC composites. *Comp Sci Technol* 2007;**67**:1009–17.
18. Morscher GN, Ojard G, Miller R, Gowayed Y, Santhosh U, Ahmed J, John R. Tensile creep and fatigue of Sylramic-iBN melt-infiltrated SiC matrix composites: retained properties, damage development, and failure mechanisms. *Comp Sci Technol* 2008;**68**:3305–13.
19. Morscher GN, Pujar VV. Effect of fiber-type on mechanical properties of melt-infiltrated 2D woven SiC–SiC composites. *Int J Appl Ceram Technol* 2009;**6**:151–63.
20. Yun HM. Tensile creep of Sylramic-iBN fiber. Private communication.
21. Morscher GN. Modeling the elastic modulus of 2D woven CVI SiC composites. *Comp Sci Technol* 2006;**66**:2804–14.
22. Yun HM, DiCarlo JA. Comparison of the tensile, creep, and rupture strength properties of stoichiometric SiC fibers. *Ceram Eng Sci Proc* 1999;**20**(3):259–72.
23. Sauder C, Lamon J. Tensile creep behavior of SiC-based fibers with a low oxygen content. *J Am Ceram Soc* 2007;**90**(4):1146–56.
24. Morscher GN, DiCarlo JA. A simple test for thermomechanical evaluation of ceramic fibers. *J Am Ceram Soc* 1992;**75**:136–40.
25. Morscher GN, Lewinsohn CA, Bakis CE, Tressler RE, Wagner T. A comparison of bend stress relaxation and tensile creep of CVD SiC fibers. *J Am Ceram Soc* 1995;**78**:3244–52.
26. Morscher GN, Yun HM, Goldsby J. *Bend Stress Relaxation and Tensile Primary Creep of a Polycrystalline* α*-SiC Fiber, Plastic Deformation of Ceramics*. NY: Plenum; 1995. pp. 467–478.
27. Youngblood GE, Jones RH, Morscher GN, Kohyama A. Creep behavior for advanced polycrystalline SiC fibers, in *Fusion Materials Seminannual Progress Report for Period Ending June 30, 1997*, DOE/ER-0313/22 p. 81ff.
28. Sha JJ, Park JS, Hinoki T, Kohyama A. Bend stress relaxation of advanced SiC-based fibers and its prediction to tensile creep. *Mech Mater* 2007;**39**:175–82.
29. Morscher GN. Unpublished data.
30. Morscher GN. Tensile creep of melt-infiltrated SiC/SiC composites with unbalanced Sylramic-iBN fiber architectures. *Int J Appl Ceram Technol*, in press.

31. Hill BB, Bakis CE, Hahn HT. Creep of SiC/RBSN composite: analytical modeling. In: *MD-Vol 40 Constitutive Behavior of High-Temperature Composites ASME*. 1992. p. 121–35.
32. Park YH, Holmes JW. Finite element modeling of creep deformation in fibre-reinforced ceramic composites. *J Mater Sci* 1992;**27**: 6341–51.
33. Rugg KL, Tressler RE, Bakis CE, Lamon J. Creep of SiC–SiC microcomposites. *J Eur Ceram Soc* 1999;**19**:2285–96.
34. Evans AG, Zok RW. Review: the physics and mechanics of fibre-reinforced brittle matrix composites. *J Mater Sci* 1994;**29**: 849–58.
35. Guillaumat L, Lamon J. Multi-fissuration de composites SiC–SiC. *Rev Composit Mater Avan* 1993;**3**:159–71.
36. Pulvinage P, Parvizi-Majidi A, Chou TW. Damage characterization of two-dimensional woven and three-dimensional braided SiC–SiC composites. *J Mater Sci* 1996;**31**:232–41.
37. Eldridge J. Unpublished data.
38. Morscher GN, Ning XJ, DiCarlo JA, Pirouz P. Effect of heat treatment on the stress relaxation and microstructure of CVD SiC fibers. In: Bansal N, editor. *Advances in Ceramic Matrix Composites*. *Ceramic Transactions 1993*, vol. 38. 1993. p. 679–90.
39. Wiederhorn SM, Roberts DE, Chuang TJ, Chuck L. Damage-enhanced creep in a siliconized silicon carbide: phenomenology. *J Am Ceram Soc* 1988;**71**:602–8.
40. Yun HM, Wheeler D, Chen Y, DiCarlo JA. Thermo-mechanical properties of super Sylramic SiC fibers. *Ceram Eng Sci Proc* 2005;**26**:59–66.